A wide-band, single-channel acoustical probe for observations of vertical fine structure in zooplankton.

Charles F. Greenlaw and RoniSue Player, Tracor Applied Sciences, Inc., 4669 Murphy Canyon Road, San Diego, CA 92123, and Robert W. Stokes. Tracor Applied Sciences, Inc., 6500 Tracor Lane, Austin, TX 78751.

Single-frequency acoustical estimates of zooplankton biomass are notoriously inaccurate, varying 10-30 dB with variations in sizes of the scatterers. Multi-frequency acoustical estimates are much more accurate but require substantial data processing. A compromise system, utilizing wide-band acoustical signals (2.5-3.5 MHz) and broadband processing to reduce the sensitivity to scatterer size variations, has been developed. This system offers the advantages of rapid single-channel data rates and high spatial resolution while providing satisfactory accuracy in biomass estimation. System design required development of several novel subsystems: a broadband transducer with an acrylic lens for obtaining reasonable acoustic sample volumes from physically practical elements; a programmable broad-band signal generator; and a wideband square-law receiver/detector. [Work supported by ONR Oceanic Biology and NSF Biological Oceanography.]

Paper presented at the Third Joint Meeting of the Acoustical Society of America and the Acoustical Society of Japan, 2-6 December 1996, Honolulu, Hawai'i.

BACKGROUND

A simple acoustical probe has been developed to provide rapid estimates of zooplankton biomass in conjunction with a suite of optical instruments. These optical sensors had previously shown the presence of critical-scale (10's to 100's of cm in the vertical), intense layers of phytoplankton occurring in certain shear-flow regimes in the ocean. The presence of these layers suggested the possibility that zooplankton might also

aggregate in these layers to exploit the high levels of food. Thus, an acoustical probe operating on the same spatial and temporal scales as the optical instruments seemed desirable for examining these layers for the presence of zooplankton. The primary targets were copepods, principally stage IV-V copepodites on the order of 200 μ total length (TL).

Originally, we planned to adapt our existing multi-frequency TAPS (Holliday and Pieper 1995) technology by altering the transducer geometry and the data processsing method (number of frequencies per transducer, transmission bandwidths, etc.). One major constraint, however, was the desire for real-time outputs that were approximately proportional to biomass. Real-time outputs ruled out using multiple discrete-frequency channels such as used in our TAPS systems (usually 4-6 frequencies) since considerable data post-processing is required to extract size-abundances from the back-scattering data. Easily interpreted raw data outputs were deemed imperative. The need for quantitative precision was relaxed over that of TAPS instruments; in particular, only regions of fairly high zooplankton densities were of interest.

Some time was spent investigating the use of a 2-frequency system. We reconfigured a 4-frequency TAPS (which we dubbed a miniTAPS) to use just the upper two frequencies--1.1 and 3 MHz. We then tested it using our 2-frequency algorithm (Greenlaw 1979, Holliday 1994) for size/biovolume estimation. This is the simplest realization of a multi-frequency system, requiring only minor data processing (basically just table lookup and some algebra) to obtain estimates of biovolume (BV) and dominant scatterer size (ESR). Results from this MINI-TAPS were encouraging but the requirement for usable raw data outputs was not met. The data rate was also marginal for adequate vertical resolution. An important limitation was the complete loss of data whenever the dominant acoustic size fell out of the range of the 2-frequency algorithm. When the 2-frequency algorithm cannot find a size, it also cannot find a biovolume.

In order to provide a system that required no operator intervention and no post-cast data processing, we elected to take a completely different approach. It had been shown previously (Greenlaw, Johnson, and

Pommeranz 1980) that operating in the geometric-optics regime of a euphausiids' Target Strength curve results in reduced-variance estimates of biovolume for single-frequency measurements. We examined this argument for the case of copepods as scatterers--with one addition.

The target strength of a copepod is well-approximated by a truncated fluid sphere scattering model. TS is a function of both size and frequency. At a fixed frequency (3 MHz in this example), TS varies with scatter size (ESR) as shown in Fig. 1 (solid curve). Since our goal is to estimate BV, it is more instructive to look at the scattering response versus size for constant BV. This curve (Volume Scattering Strength, or Sv, for BV = 1000 mm^3 / m^3) is shown as the dashed curve in Fig. 1. It is evident that the variation in BV with size is less than the variation in abundance implied by the TS curve and, over limited ranges of size, the variation is not excessive. For example, if the dominant size of a population of copepod changed from 50 μ ESR (about 200-250 μ total length, or TL) to 100 μ ESR (400-500 μ TL) while the biovolume stayed constant, Sv would only change by about 3 dB. Put another way, for populations with dominant sizes between relatively narrow ranges, Sv at a single, carefully chosen frequency can be used to estimate changes in BV to a precision of a few dB (ca. ±50%). For many important problems this would be considered acceptable precision.

This observation suggested that it might be possible to further reduce the variation of BV with size over larger ranges by averaging over frequency. In other words, replace the implied CW acoustic signal with a broadband signal. Over reasonable ranges of ESR and for proper choices of the center frequency and bandwidth, employing broadband signals might make it possible to reduce the fluctuations to more tolerable levels.

A typical situation is shown in Fig. 2. The upper panel shows the abundance versus ESR that results in a constant biovolume of 1000 mm^3 / m^3. ESR's cover the range of interest, from roughly 200 μ TL to about 1 mm TL copepods. The lower panel shows the output of a broadband system for several values of acoustical signal bandwidth ranging from essentially zero to 3 MHz. The center frequency is 3 MHz in all cases. Acoustical outputs are in

arbitrary units, expressed in dB. Of interest here are only the relative levels at different ESR's.

For a CW signal of 300 μSec duration, the variation in output for size variations over a fairly broad 5:1 range in dominant size is ±7.2 dB. Using a 1 MHz bandwidth signal reduces this to ±4.8 dB and a 3 MHz bandwidth reduces the variation to about ±2.4 dB. These are useful reductions if a practical acoustical system can be designed with these wide bandwidths.

Of course, increasing system bandwidth is not without penalty. At a minimum, both the acoustic and electronic noise levels are increased proportionately with bandwidth. We selected the 1.0 MHz bandwidth as a practical compromise between receiver noise and sensitivity to size variations. The center frequency, 3.0 MHz, used in Figs. 1-2 was selected in part by the fact that we had suitable broadband transducer elements on hand.

PROTOTYPE SYSTEM DESIGN

The block diagram (Fig. 3) of the wide-band high-resolution acoustic probe electronics consists of four major assemblies: a transmitter with a versatile, programmable gated oscillator; a broadband reciever with contollable gain; the transducer; and a controller unit with a CPU and ancillary measurement capability.

TRANSMITTER

We have developed an efficient push-pull, transformer-coupled power amplifier for portable sonars that is used in most of our battery-powered multi-frequency systems. It consists of a stable crystal oscillator feeding a digital gating circuit which in turn drives the gates of two power V-FET's. The V-FET's alternately ground the two primary windings of a push-pull transformer; the center tap is supplied with +15V from a large storage capacitor. The output winding is designed to deliver >100 W into 50 Ω from 100 KHz to over 5 MHz at pulse lengths up to about .5 mSec (depending on

rep rate). This transmitter design was employed for the new system, save for the crystal oscillator.

Since the prototype signal was a LFM sweep, we required a tunable oscillator that could be easily swept over 1 MHz or more in about .3 mSec. Various digital synthesizers are available which can be set to generate linear sweeps or discrete frequencies but none were found that met all of our requirements for power consumption, speed, versatilty, and ease of use. Eventually, we decided to design a programmable oscillator around a current-controlled oscillator chip (MAX038, Maxim Integrated Products, Inc.). Simple gating logic controls an up-counter with 9 bits of parallel output. These outputs are connected to the lower 9 address lines of an EPROM. The 8 data bits of the EPROM drive a Digital-to-Analog Converter (DAC) to produce a voltage proportional to the 512 sequential data words read out of the EPROM. The DAC output drives a voltage-to-current converter which in turn varies the output frequency of the oscillator.

Two additional address lines were routed to the controller card to permit selection of particular transmit codes by the user. A third address line is switch-selectable on the board to allow changing to a different repertoire of signals.

This simplest signals are CW. The code for this is 512 consecutive words of one fixed value. Several test signals were provided in the EPROM to permit testing and calibration.

The prototypical signal is a LFM sweep from 2.5 to 3.5 MHz. The code for this consists of 256 pairs of values ranging from 00 to 255, giving a stepped-FM analog of the LFM prototype.

The analysis that suggested the use of wideband signals implied the use of a flat spectrum signal. Measurements of system sensitivity showed a clear peak in system response at 3.25 MHz and about 9 dB variation over the band. Rather than attempt to design a passive equalizer circuit to flatten the transducer response, we elected to modify the drive signal to achieve a flat system response. The simplest way to accomplish this was to adjust the

sweep rate of the FM signal to produce equal intensity in each frequency 'bin across the signal. Using this drive signal, the expected echo spectrum from a perfect, frequency-independent target would be rectangular with a 1 MHz bandwidth.

We fit a smooth curve to the measured system response data and sampled this curve at 25 KHz (Fig. 4 upper panel). The relative response was then inverted to convert the relative system sensitivity into a relative length of time the system should dwell at each frequency to obtain equal energy at each frequency (Fig. 4 lower panel). These dwell times were then scaled to numbers of data words in the 512 word memory of the EPROM. This equal-energy signal was employed in most of the field testing.

An even better signal might be one that also includes the change in sample volume versus frequency, although this effect was small with the transducer we used. This signal has not been employed to date.

As an example of a slightly different application, we could even account for the expected TS response of the target organisms in the transmit signal, enhancing the response for a selected size class of scatterer. This signal would combine the equal-energy approach, to account for system response, with the backscattering response expected from the selected scatter. This should produce a system 'tuned' to a particular size-class of scatterer. The resolution of such a system in size-abundance space has not been analyzed but it is expected that the tuning curve would not be especially sharp because the shape of the Sv curve (Fig. 1) is not highly peaked.

RECEIVER

Several approaches to receiver design were examined -- a SAW-based matched-filter receiver, a tracking-filter design, and a simple broadband receiver were among the candidates. The latter proved to be the simplest approach and was the one implemented (although we had initial concerns about signal-to-noise limitations).

With simple broadband transmission/reception, the instantaneous echo intensities are proportional to the integral of backscattered intensity over the pulse duration--assuming sufficient density of scatterers--and need no further processing to represent a point estimate of the volume scattering process.

To obtain the best noise figure possible, we elected to use a commercial preamp (Panametrics, Inc.) with known specifications as the first gain stage. Broadband noise was advertised as < 15 μVp-p RTI over the .5-10 MHz bandwidth of the amplifier. This stage was followed by a custom passive bandpass filter with a 1.5 MHz bandwidth and two stages of low-noise amplification. A controllable 0-30 dB attenuator was inserted between the second and third gain stages to permit automatic adjustment of gains to account for signal levels.

The major design impediment for this application was designing a linear detector with adequate dynamic range that would work at MHz frequencies. This proved to be an intractable problem so we cheated by using a wideband multiplier and an RC output filter to generate echo intensities directly from the squared echoes. While this approach worked well in bench tests, it effectively doubled the required dynamic range of the ADC. A signal that varies over a 256:1 range produces squared outputs that vary over a 65536:1 range. Since we needed to sample at a rather pedestrian rate of 6.6 KHz, we could employ a not-especially-speedy 16-bit ADC to sample these signals . This still provided only the equivalent of an 8-bit converter operating on signal amplitudes.

This was considered an acceptable tradeoff if we could ensure that signal levels were maintained within the dynamic range of the converter. Thus the addition of the 30 dB switched attenuator to the receiver. We put an AGC routine in the CPU code to keep the echo signals within a reasonable range, yielding a theoretical effective dynamic range of the receiver system approaching 76 dB (although noise limits the real dynamic range to approximately 60-65 dB).

TRANSDUCER

We selected 3 MHz as the center frequency, in part because suitable transducer elements were on hand. A 1 MHz bandwidth was deemed a practical maximun system bandwidth, at least for the prototype system where noise levels were problematic. For planning purposes, we envisioned a linear-frequency-modulated (LFM) transmit signal.

An ideal pattern for our transducer, at least for use in cast-mode, would be one which is omnidirectional in azimuth and narrow in elevation, thus giving maximum vertical resolution while still providing a large sample volume to ensure adequate numbers of scatterers on each ping. A cylindrical element provides this sort of pattern but the losses due to diffraction are as much as 20 dB one-way, precluding its use in this application.

Consideration was also given to using a cylindrical segment transducer (Stokes, Smith, and Mellenbruch 1976). It was believed that this might reduce the diffraction losses to an acceptable level without reducing the effective ensonified volume too severely. Several test elements were constructed from broken 1140 KHz cylinders on-hand and tested. The basic cylindrical segments behaved as expected, showing higher sensitivity than the complete cylinders due to lower diffraction losses and yielding azimuthal patterns similar in extent to the angular extent of the segment, although with considerable scalloping within the main lobe. Vertical patterns were less satisfactory, showing sidelobes as high as -5dB. Attempts at pattern control included scalloping the edges of the back electrode and reducing the width of the back electrode to emulate the linear gaussian source developed by Martin and Brazeale (1971). Results were not particularly encouraging so no effort was made to build similar transducers at the (higher) operating frequency selected for the actual system.

Instead, we turned our attention to one-dimensional patterns from circular-piston transducers. There are several ways in which a broader beam may be generated from a circular-piston transducer of fixed size. One scheme (Du and Breazeale 1985) utilizes a reduced diameter electrode on one surface to produce an approximately-gaussian fringing electric field in the ceramic,

resulting in a nearly gaussian beam pattern. Transducers we have built using this scheme have no discernible loss in efficiency--although there is a loss in sensitivity due to the decreased directivity index--and useful -3dB beamwidths of 8-12° are easily achieved. The impedance is increased, sometimes to awkward levels, but we have seen no other deleterious results. This design is used in the TAPS units at 1.1 MHz and above.

An alternative modification that does not effect either the efficiency or the impedance of the piston element involves cementing a convex acrylic lens to the radiating face of the transducer. We experimented with various sizes of lenses (both radius of curvature and segment height) to obtain beam patterns of various sizes.

Two transducers were built for testing; The first utilized a simple circular-piston element with no shading or other attempt at beam control. The second was similar except for the addition of the small acrylic lens cemented to the radiating face. The elements were cemented in a cup-shaped aluminum housing that was filled with silicone oil. A thin plastic membrane (Handywrap) was used as an acoustic window. An LC matching network designed to provide approximately 50 Ω impedance over the 2.5 - 3.5 MHz band was installed in a rear chamber of the transducer housing. Coax cable with water-tight connectors was used to connect the transducers to an electronics package.

The transducer elements we used were cylindrical disks of piezo-ceramic, series resonant at 3 MHz, with lossy sintered-bronze backings. These elements had been tested for use in a deep-submergence TAPS unit with good results. The diameter was 12.7 mm, giving a mid-band directivity index of about 37 dB for the unshaded element, rather higher than desired or needed. The -10 dB beamwidth of the beam from this transducer is about 5°. At a range of 80 cm, the cross-range extent is about 7 cm. Using a pulse length of 300 μSec the sample volume at 80 cm would be about 190 ml. This implies a lower limit on scatterer density for this transducer of > 5000/m^3. While not necessarily a low value of abundance for the small copepods of interest, this small sample size does limit its use to regions of fairly intense biomass.

The second transducer utilized a 1.8mm high segment from a 25.4mm diameter acrylic sphere as a convex de-focussing lens. Preliminary broadband measurements of this element suggested a beamwidth of about 10° with no sidelobes visible near the mainlobe. The impedance was well-behaved and exhibited no resonances in the 2.5-3.5 MHz band. After installation in a housing and attachment of a tuning network, beam patterns were measured at discrete frequencies from 2.5 - 3. 5 MHz. These data showed much higher beamwidths (<DI> = 20.8 dB; -10 dB beamwidth of 30°) with noticeable scalloping of the main lobe. Interestingly, even though the patterns were unique at each frequency, the DI varied only ±1 dB over the 2.5 - 3.5 MHz frequency range. Because we were unable to explain the differences in the preliminary and final transducers, and due to time constraints, we elected to do our initial testing with the narrow-beam transducer almost exclusively.

CONTROLLER

Although this sensor was intended to be used in conjunction with CTD's which would provide depth and physical properties context for the acoustic data, it seemed prudent to add depth and temperature sensors so that the unit could be used in stand-alone applications as well.

Temperature is sensed via a 7 mS response thermistor housed in a small PVC case that can be mounted in close proximity to the transducer. A bridge circuit converts the thermistor resistance to a voltage. This voltage is amplified and connected to the 16-bit ADC via a MUX.

Depth is estimated from a pressure sensor mounted in the electronics case endcap. The sensor comprises a strain gauge bridge that outputs a voltage proportional to pressure. This voltage is amplified and also connected to the ADC via a MUX.

A simple 68HC11 single-board-computer is sufficient to control system functions and provide serial data communications to the user. This card generates the signals to select the transmit program and to control the MUX.

Transmit triggers are generated by the SBC and, following a programmable delay, samples of the echo intensity are measured.

Data lines consist of time (from a real-time-clock) in hours, minutes, and seconds to permit synchronization of this data with other instruments; a code value that contains the transmit signal program number and the receiver attenuator setting; raw binary values of depth and temperature; and the sum of N samples on M pings of broadband echo intensity. Typically, N = 4 samples per ping and M = 3 pings per output.

PRELIMINARY DATA

A typical profile obtained with the prototype system is shown in Fig. 5; the data are from San Vicente Reservoir, a man-made fresh-water lake located close to our San Diego laboratory. The left panel shows the temperature structure versus depth. As is typical for summertime in Southern California, there is a strong thermocline below a well-mixed surface layer. The device output, in arbitrary units, is shown in the right panel. Dots denote the individual outputs (at 4 samples per ping and 3 pings per output) while the solid line was obtained by binning data into 20 cm depth bins. The shape of the average curve is certainly plausible, with structure both above and below the thermocline and interesting details within the thermocline.

The distribution of individual data points was investigated in some detail to determine whether the binned averages fairly represented the raw data, as some data sets suggested that some of the highest values might represent rare instances of scattering from larger organisms. Comparisons with filtered theoretical pdf's showed that these higher values were consistent with the expected outcomes for volume scattering, however, and thus that the binned data were valid estimates of the mean scattering intensity. This does not exclude the possibility that useful information exists in the tails of the echo intensity distributions but this notion has not been investigated further at this time.

The prototype system was tested several times at this reservoir. One test consisted of comparing the outputs of the prototype to the estimated biovolumes obtained from the miniTAPS system. About 30 minutes prior to this test we deployed a 6-frequency TAPS unit to obtain a vertical profile. Estimates of biovolume versus depth obtained from the TAPS are shown in the left-hand panel of Fig. 6. There is a strong layer at about 10m with relatively low biovolume above this layer and somewhat higher biovolume below it. The size-abundances, shown in the right-hand panel of Fig. 6, show that the biomass is dominated by small (<50 μ ESR or <200 μ TL) organisms above and below the 10m layer and by somewhat larger (100 μ ESR or 400 μ TL) organisms within the layer. A few larger scatterers are found in and above this layer. Note that the sample volume of this TAPS is .001m^3, some five times that of the wideband system prototype.

The prototype and the miniTAPS were lowered together to produce the vertical profiles shown in Fig. 7. The miniTAPS estimates of biovolume agree rather well with the 6-frequency TAPS estimates in both shape and level. The prototype system output was scaled by eye to match the miniTAPS profile within the main layer. Within and below the main layer, the fit is excellent. Above about 6m, the wideband system output is lower than the biovolume estimated by miniTAPS but it shows structure that leads one to wonder if the wideband system result is not more likely correct. The amount of the discrepancy is within the expected precision of the prototype (although the preceeding TAPS cast suggests there are no size differences above and below the layer to cause biovolume estimation errors). This may indicate that the prototype system has a better noise floor than the miniTAPS unit.

Comparisons among acoustical instruments are not entirely satisfactory proof of performance. Therefore we conducted a test comparing the wideband system outputs to biovolumes measured from samples taken using a 2" plankton pump at several depths. Unfortunately, this test could not be conducted until early November when peak biovolumes had declined precipitously. The comparisons, however, were satisfactory as shown in Fig. 8. The dominant zooplankters were calanoid copepods with ESR's varying from .1 to .13 mm. A few cyclopoid copepods and cladocerans were also observed; the ESR's of these organisms were smaller yet. The limited range

of biovolumes available and the small variation in sizes present a relatively weak test for the wideband system concept but the agreement over the ranges available, combined with the results of the comparison to the miniTAPS, suggest that the system has met its basic goal of providing an output proportional to zooplankter biomass.

During the test period prior to the pump tests, the opportunity was taken to obtain a time-series of data using the wideband prototype system. We tied up to a marker buoy in some 46m of water near the dam and outflow. The device was slowly lowered and raised continuously for 3 hours while the data were recorded. The results are shown in Figs. 9-10. Figure 9 shows the evolution of temperature over time beginning at 0900 PST. The sharp thermocline (cf Fig. 5) is evident throughout with some evidence of small-scale structure visible.

The zooplankton structure inferred by the wideband prototype system is shown in Fig. 10. The color scale represents the logarithm of biovolume. While the relatively thin main layer persists over the entire record, there is clear evidence of smaller-scale structure both within, above, and below this layer. Since the horizontal current structure was not known during this experiment, no sizes can be inferred for the small-scale patches that appear and disappear in this figure. One has confidence from the preceeding data, however, that these features are real.

REFERENCES

Du, Gonghuan and M. A. Breazeale, 1985. The ultrasonic field of a Gaussian transducer. J. Acoust. Soc. Am. 78(6): 2083-2086.

Greenlaw, C. F., 1979. Acoustical estimation of zooplankton populations. Limnol. Oceanogr. 24: 226-242.

Greenlaw, C. F., R. K. Johnson, and T. Pommeranz, 1980. Volume scattering strength predictions for Antarctic krill (Euphausia superba Dana). Meeresforsung 28:48-55.

Holliday, D. V., 1977. Extracting bio-physical information from acoustic signatures of marine organisms. *In* Ocean sound scattering prediction, pp 619-624. Ed. by N. R. Andersen and B. J. Zahuranec. Plenum Press, N.Y. 859 pp.

Holliday, D. V., 1994. Zooplankton population density assessment with acoustics. J. Acoust. Soc. Am. 96(A): 3315-3316.

Holliday, D. V. and R. E. Pieper, 1995. Bioacoustical oceanography at high frequencies. ICES J. mar. Sci. 52: 279-296.

Martin, F. D. and M. A. Breazeale, 1971. A simple way to eliminate diffraction lobes emitted by ultrasonic transducers. J. Acoust. Soc. Am. 49: 1668-9.

FIGURE CAPTIONS

1. Variation of scattering strength versus scatterer size at a fixed frequency (3 MHz). The solid curve is the target strength (TS) for an individual scatter predicted from the truncated fluid sphere model. The dashed curve is the volume scattering strength predicted from the same model for a biovolume of 1 mm^3 / m^3. Axes are decibels (dB) and equivalent spherical radius (ESR) in mm.

2. Upper: numbers of scatterers required to obtain 1000 mm^3 / m^3 biovolumes versus ESR.
   Lower: volume scattering strength versus ESR for BV=1000 mm^3 / m^3 at various values of signal bandwidth (in MHz).

3. Wideband system block diagram.

4. Upper: prototype system calibration results. System gain is source level plus receive sensitivity plus gain in dB.
   Lower: relative dwell times to produce an equal-energy system response sampled at 25 KHz intervals.

5. Typical output from the wideband prototype system. Temperature versus depth shown in left panel. Intensity outputs shown in right panel as raw data (dots) and 20cm binned data (solid line).

6. Vertical structure of biovolumes as estimated by a 6-frequency TAPS. Total biovolume versus depth shown in left panel. Biovolumes as a function of ESR and depth are shown in right panel.

7. Comparison of the wideband prototype outputs and miniTAPS total biovolume estimates. Wideband system values in aribitrary units, scaled to match miniTAPS estimates at the peak.

8. Comparison of biovolumes measured from samples taken with a 2" plankton pump to wideband system outputs (raw values).

9. Temperature versus depth from a 3 hour continuously-profiled data set taken at San Vicente Reservoir.

10. Wideband system relative biovolume estimates from a 3 hour continuously-profiled data set taken at San Vicente Reservoir.

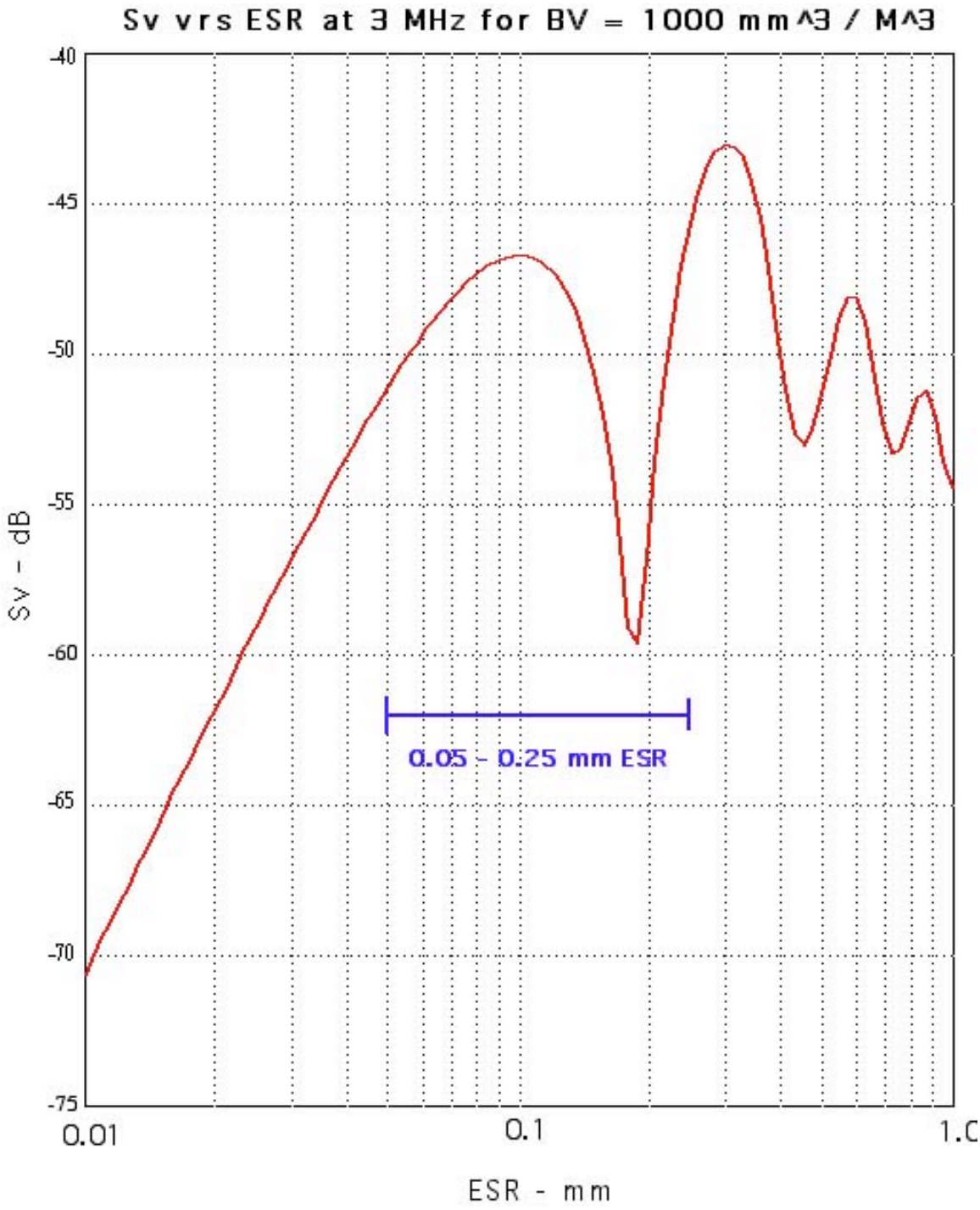
Sv vrs ESR at 3 MHz for BV = 1000 mm^3 / M^3
-40
-45
-50
-55
-60
-65
-70
-75
Sv - dB
0.05 - 0.25 mm ESR
0.01
0.1
1.0
ESR - mm

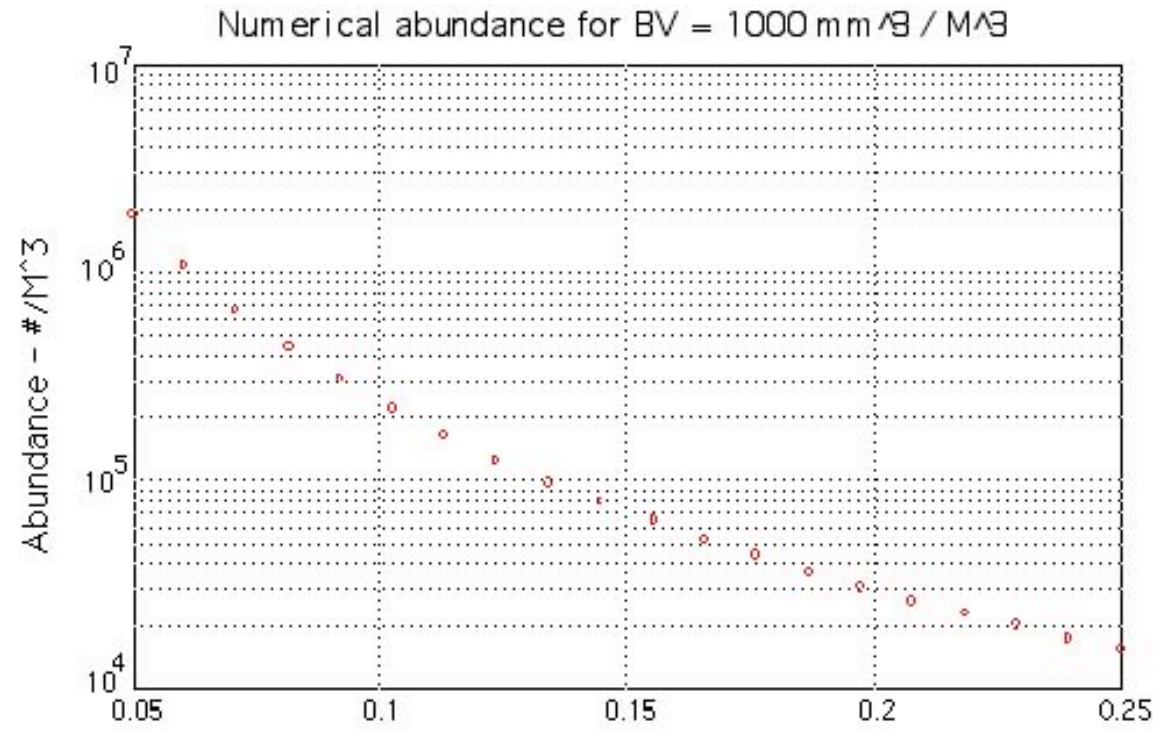
Numerical abundance for BV = 1000 mm^3 / M^3
Abundance - #/M^3
10^7
10^6
10^5
10^4
0.05
0.1
0.15
0.2
0.25

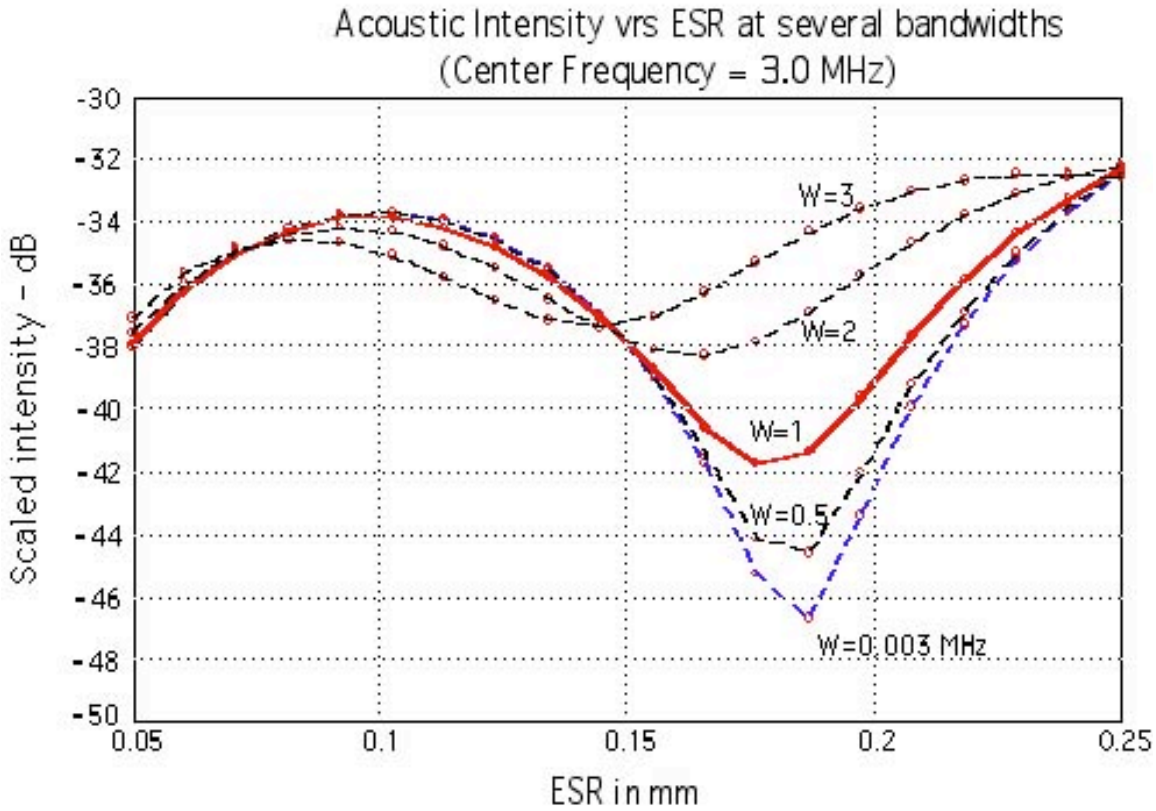
Acoustic Intensity vrs ESR at several bandwidths
(Center Frequency = 3.0 MHz)
Scaled intensity - dB
-30
-32
-34
-36
-38
-40
-42
-44
-46
-48
-50
W=3
W=2
W=1
W=0.5
W=0.003 MHz
0.05
0.1
0.15
0.2
0.25
ESR in mm

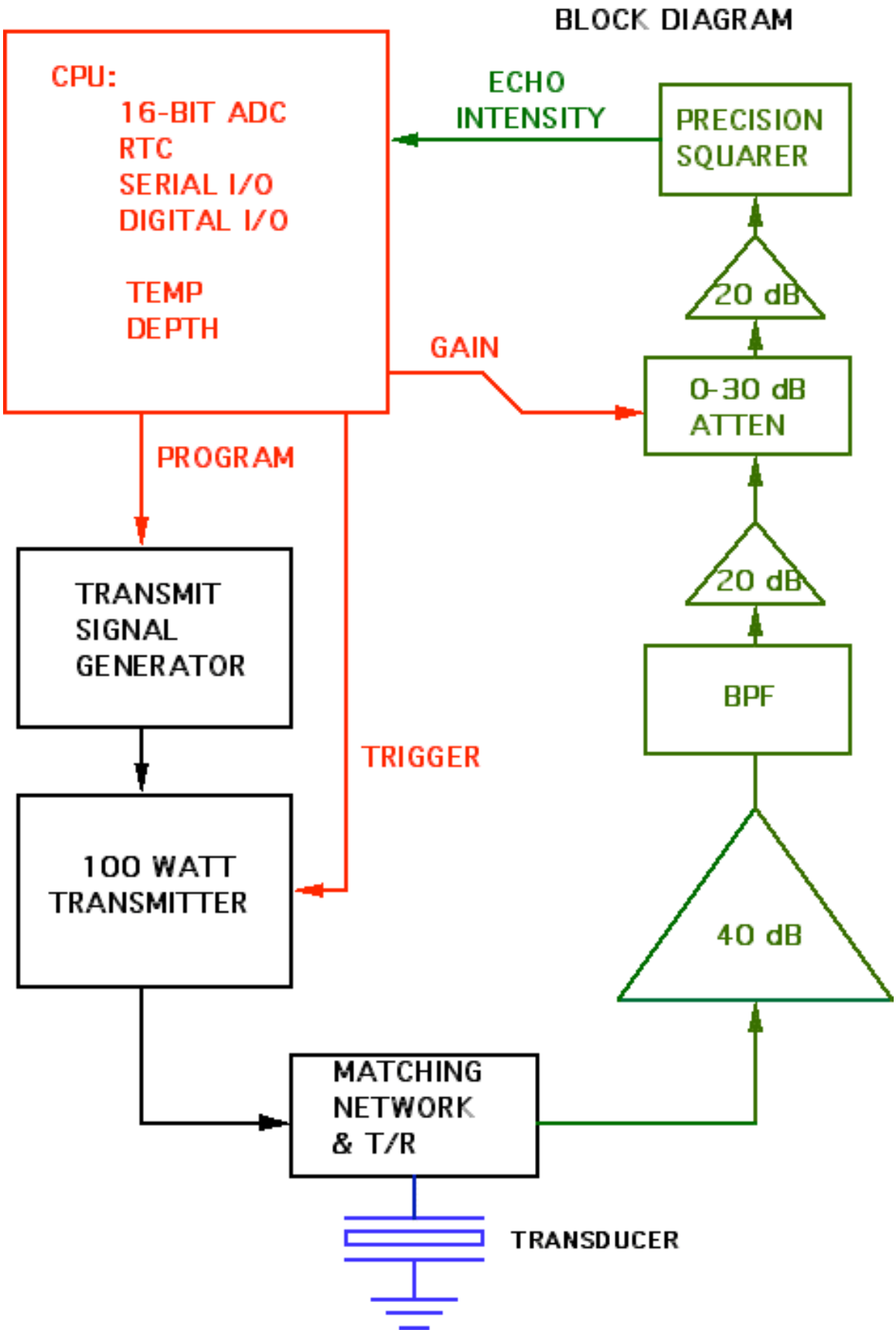
BLOCK DIAGRAM
CPU:
16-BIT ADC
RTC
SERIAL I/O
DIGITAL I/O
TEMP
DEPTH
ECHO
INTENSITY
PRECISION
SQUARER
20 dB
GAIN
0-30 dB
ATTEN
20 dB
BPF
40 dB
PROGRAM
TRANSMIT
SIGNAL
GENERATOR
TRIGGER
100 WATT
TRANSMITTER
MATCHING
NETWORK
& T/R
TRANSDUCER

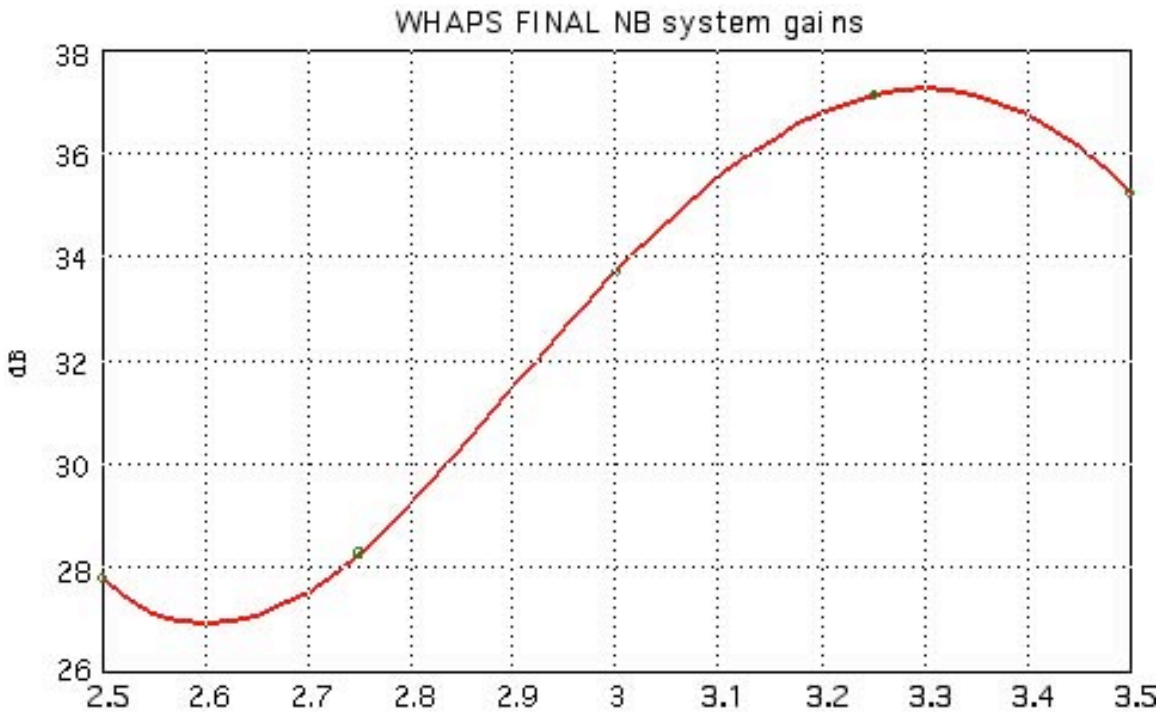
WHAPS FINAL NB system gains
dB
38
36
34
32
30
28
26
2.5
2.6
2.7
2.8
2.9
3
3.1
3.2
3.3
3.4
3.5

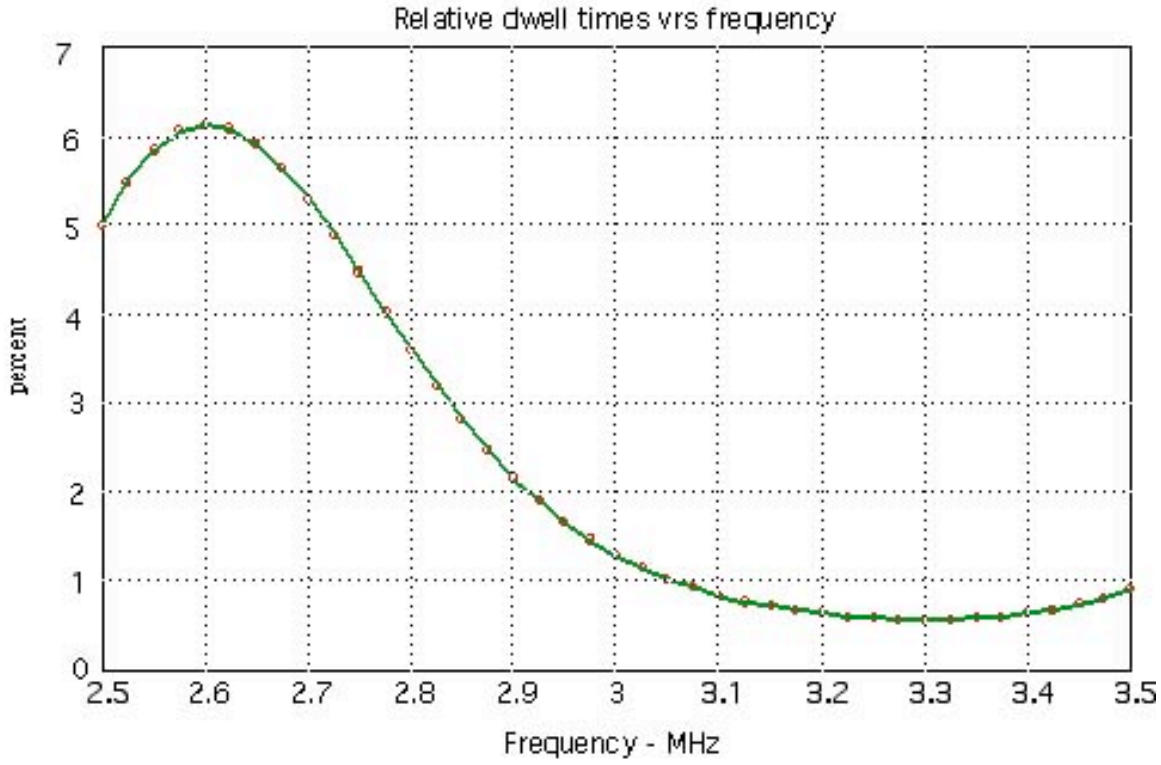
Relative dwell times vrs frequency
Percent
7
6
5
4
3
2
1
0
2.5
2.6
2.7
2.8
2.9
3
3.1
3.2
3.3
3.4
3.5
Frequency - MHz

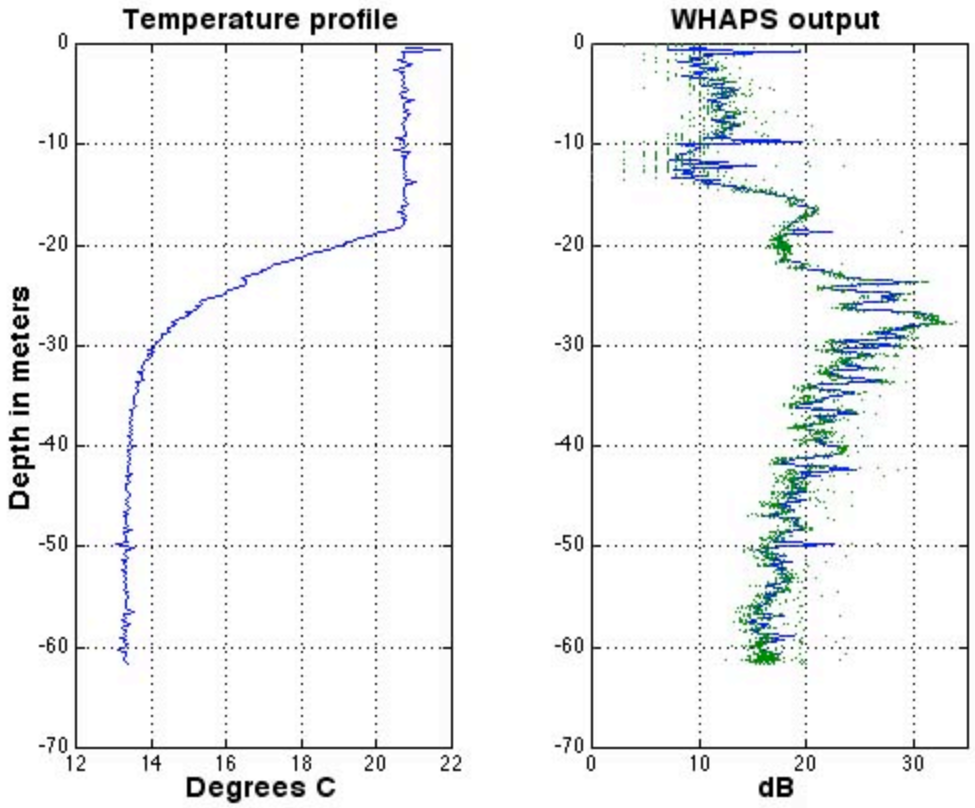
Temperature profile
Depth in meters
Degrees C
0
-10
-20
-30
-40
-50
-60
-70
12
14
16
18
20
22
WHAPS output
dB
0
10
20
30

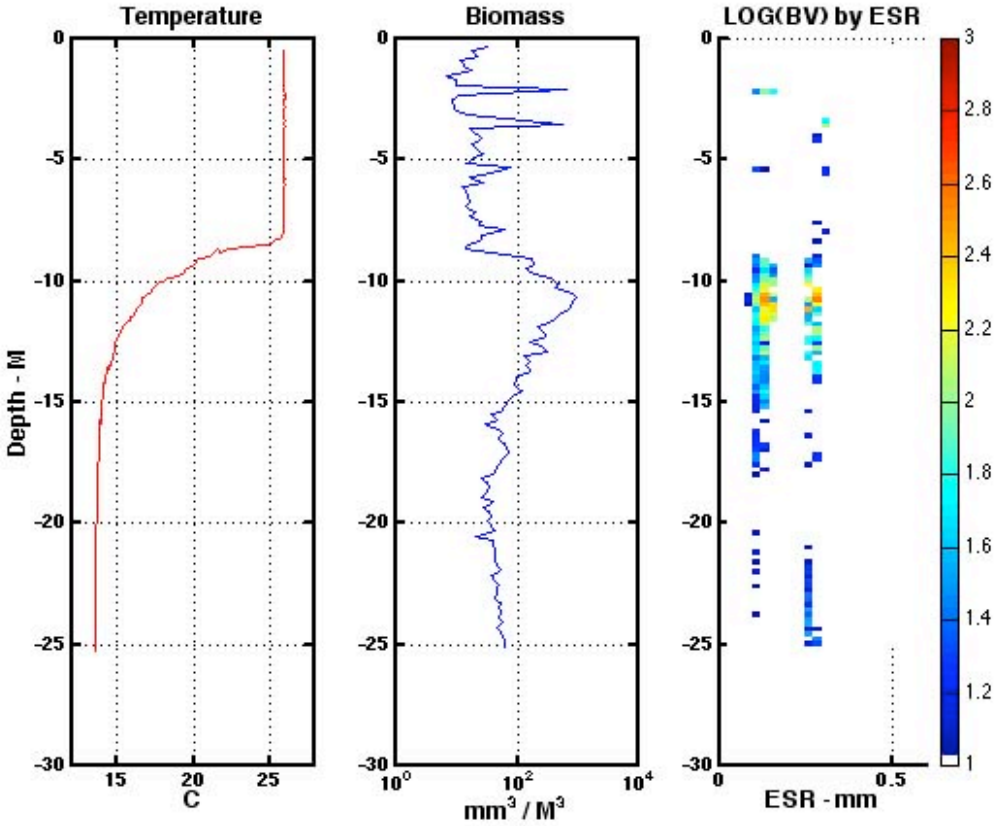
Temperature
Biomass
LOG(BV) by ESR
Depth - M
0
-5
-10
-15
-20
-25
-30
15
20
25
C
10^0
10^2
10^4
mm^3 / M^3
0
0.5
ESR - mm
3
2.8
2.6
2.4
2.2
2
1.8
1.6
1.4
1.2
1

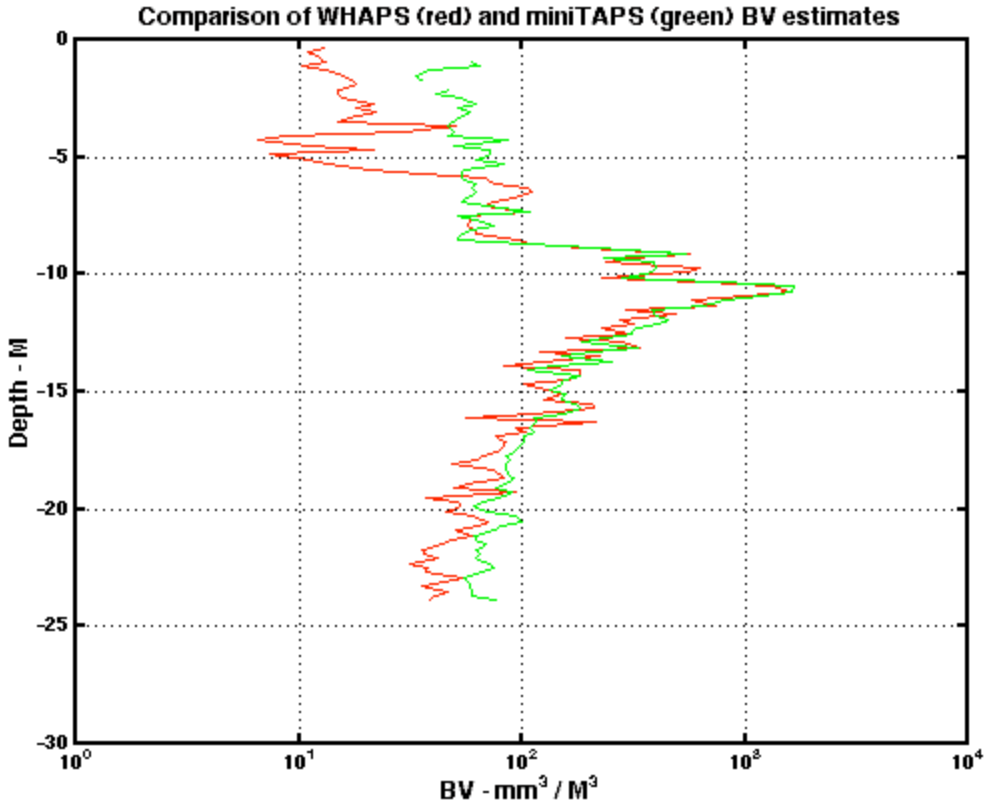
Comparison of WHAPS (red) and miniTAPS (green) BV estimates
Depth - M
0
-5
-10
-15
-20
-25
-30
10^0
10^1
10^2
10^3
10^4
BV - mm^3 / M^3

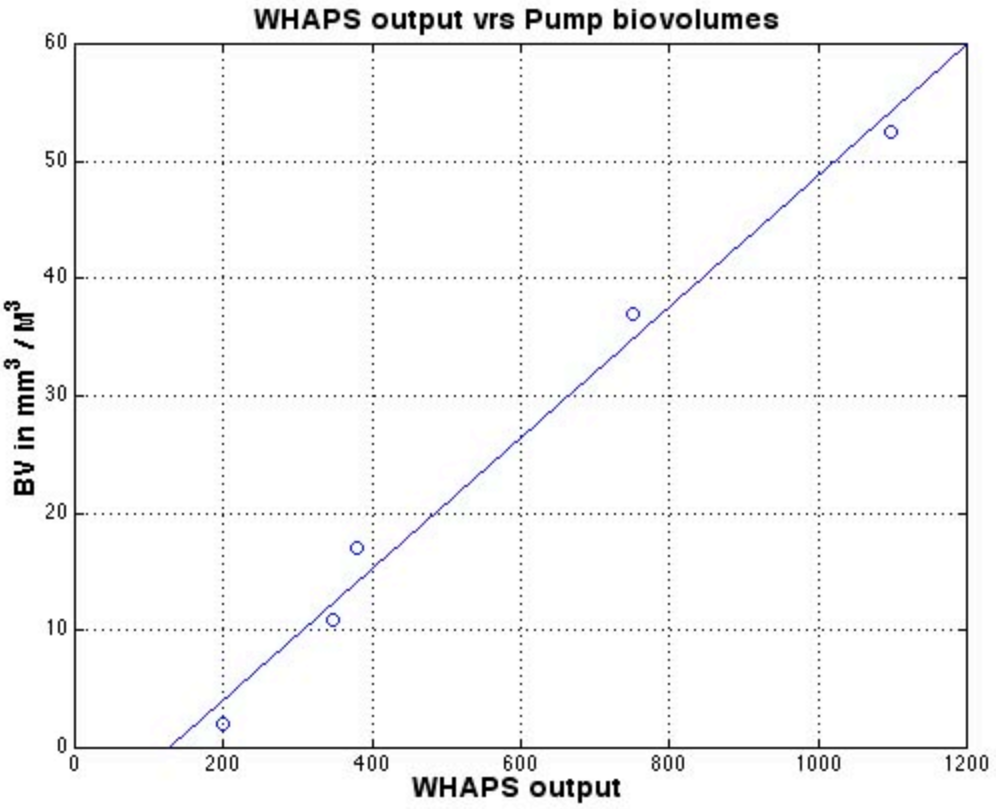
WHAPS output vrs Pump biovolumes
BV in mm3 / M3
WHAPS output
0
10
20
30
40
50
60
0
200
400
600
800
1000
1200

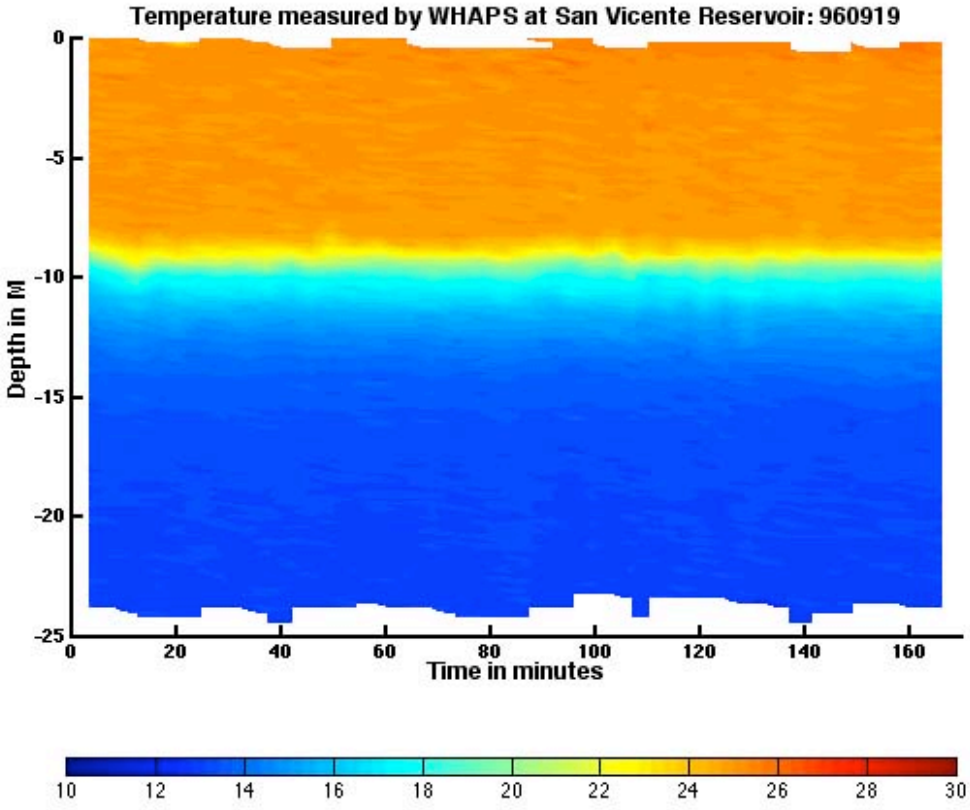
Temperature measured by WHAPS at San Vicente Reservoir: 960919
Depth in M
0
-5
-10
-15
-20
-25
0
20
40
60
80
100
120
140
160
Time in minutes
10
12
14
16
18
20
22
24
26
28
30

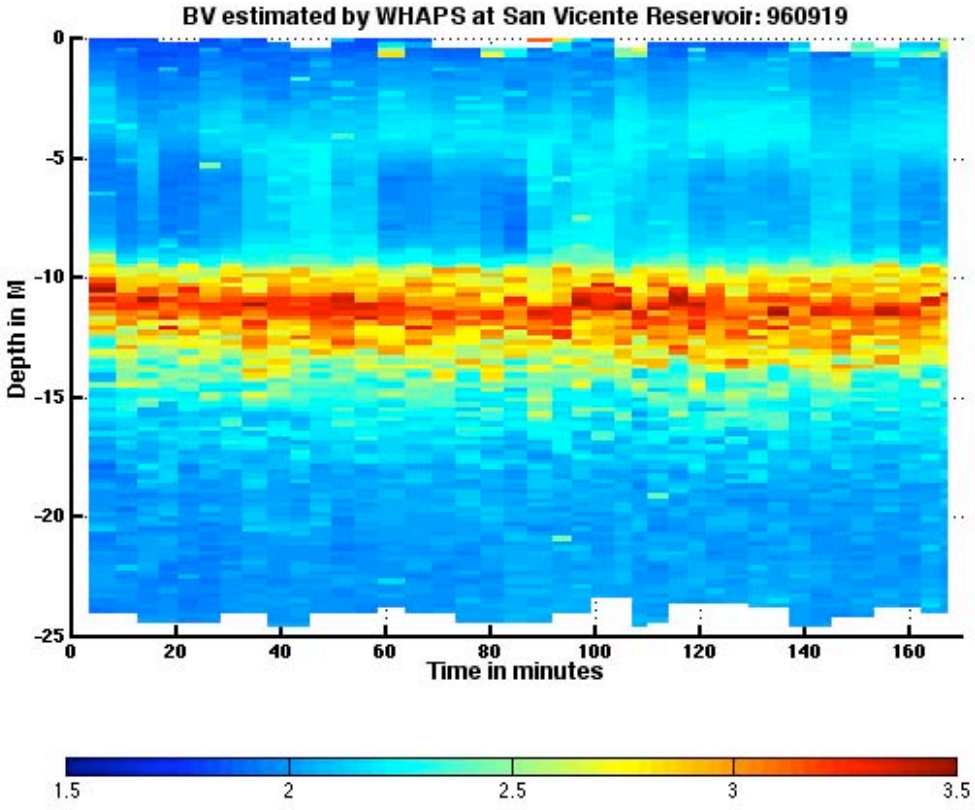
BV estimated by WHAPS at San Vicente Reservoir: 960919
Depth in M
0
-5
-10
-15
-20
-25
0
20
40
60
80
100
120
140
160
Time in minutes
1.5
2
2.5
3
3.5